UCLA
Adaptive Optics for Extremely Large Telescopes 4 – Conference Proceedings

Title
Adaptive Optics Point Spread Function Reconstruction at W. M. Keck Observatory in Laser & Natural Guide Star Modes : Final Developments

Permalink

Journal

Authors
Jolissaint, Laurent
Ragland, Sam
Wizinowich, Peter

Publication Date
2015

DOI

Copyright Information

Peer reviewed

Adaptive Optics Point Spread Function Reconstruction at W. M. Keck Observatory in Laser & Natural Guide Star Modes : Final Developments

Laurent Jolissaint[a], Sam Ragland[b], and Peter Wizinowich[b]

[a] University of Applied Sciences Western Switzerland, 1401 Yverdon-les-Bains, Switzerland;
[b] W. M. Keck Observatory, 65-1120 Mamalahoa Hwy, HI 96743 Kamuela, USA

ABSTRACT

We present the final development of our point spread function reconstruction algorithm for the Keck-II telescope adaptive optics system, in laser and natural guide star modes. The method makes use of AO loop telemetry, nearby C_N^2 profiler data, and on-sky phase diversity. We describe the fundamental assumptions and the mathematical models for each components of the residual phase structure function. The reconstructed PSF is compared with on-sky single star PSF. We emphasize the importance of access to a good telemetry and the fact that non-common path aberrations also affects PSF-R. The global, statistical quality of the reconstructed PSF demonstrates the validity of the method. The algorithm is now ready for AO science data reduction (see the companion overview paper, Ragland et al.[1] - this conference).

Keywords: adaptive optics, laser guide star, point spread function reconstruction, adaptive optics calibration, adaptive optics telemetry, W. M. Keck Observatory

1. INTRODUCTION

Reducing adaptive optics (AO) data often requires the knowledge of the point spread function (PSF) associated to the AO run. Due to the sensitivity of the AO system performance to the optical turbulence conditions (seeing), the fast variation of these conditions, and the complexity of the PSF structure, it is not possible to build a generalist PSF model that would represent any AO PSF. Getting the PSF from the image of a point source recorded before/after the AO run would be a natural option, but the seeing changes too rapidly and pre/post-run PSF are of limited interest. An ideal situation occurs when a bright, isolated star image is available close to the science object, inside the isoplanatic patch, but this case is rare in practice. A general method, independent of the field and the seeing conditions, is therefore required.

Véran et al.[2] have successfully demonstrated a PSF reconstruction (PSF-R) technique based on the AO loop data. The concept is simple : first, the wavefront sensor (WFS) measures the low order[*] residual wavefront, so it must be possible to evaluate from these measurements the contribution of the residuals to the long exposure PSF; second, as the deformable mirror (DM) is set to compensate the incoming turbulent wavefront, it must be possible to determine, from the DM commands statistics, the seeing parameters associated to the run, and, in turn, evaluate the amplitude of the high order uncorrected aberrations that went through the system. This idea was developed by Véran et al. for a curvature sensing WFS AO system and tested on PUEO, at the CFHT telescope. Later, we have adapted the method for the Shack-Hartmann (SH) WFS and tested it on ALTAIR, the Gemini-North AO system.[3] In this paper, we present our work on the final development of a PSF-R algorithm for the W. M. Keck Observatory (WMKO) AO system, a SH-based system, in natural (NGS) and laser (LGS) guide star modes.

Further author information: e-mail: laurent.jolissaint@heig-vd.ch
[*]these are the modes (Zernike, Influence Functions etc.) that can be sensed and corrected by the system; high order modes are all the others : the turbulent aberrations at spatial frequencies above the system cutoff frequency 0.5/pitch.

2. SUMMARY OF THE PSF-R METHOD APPLIED TO KECK AO SYSTEM

2.1. The core of the method

This part is common to the NGS and LGS modes. The focal anisoplanatism structure function, specific to the LGS, is discussed further. For details, see Refs. 1-8. Assuming that the residual phase is stationary inside the telescope pupil, it can be shown that the long exposure optical transfer function (OTF) can be written as the product of a static OTF (telescope and instrument) and an AO-OTF

$$\text{OTF} = \text{OTF}_{\text{tel}} \cdot \text{OTF}_{\text{AO}} \tag{1}$$

the long exposure PSF is computed from the reconstructed OTF, applying an inverse FFT algorithm. The AO-OTF is related to the long exposure residual phase structure function, which can be split in two components, the low order residual aberrations (actually split into the DM modes and the tip-tilt), and the high order, unsensed and uncorrected aberration (the cross-term is assumed negligible)

$$\text{OTF}_{\text{AO}}(\boldsymbol{\nu}) = \exp\left[-\frac{1}{2}\overline{D}_\varphi(\lambda\boldsymbol{\nu})\right] \quad \text{with} \quad \overline{D}_\varphi(\lambda\boldsymbol{\nu}) = \overline{D}_{\text{L}}(\lambda\boldsymbol{\nu}) + D_{\text{TT}}(\lambda\boldsymbol{\nu}) + \overline{D}_{\text{H}}(\lambda\boldsymbol{\nu}) \tag{2}$$

where $\boldsymbol{\nu}$ is the angular frequency vector on the sky, $\lambda\boldsymbol{\nu} = \mathbf{r}$ is the coordinate vector inside the pupil, and the bar above D indicates an average of the structure function across the pupil. The tip-tilt structure function D_{TT} is discussed later. The high-order structure function is computed from a Monte-Carlo experiment, knowing the system's modes and the optical turbulence parameters associated to the run (seeing and outer scale, see below). The low order structure function is computed from

$$\overline{D}_{\text{L}}(\lambda\boldsymbol{\nu}) = \frac{1}{\mathcal{A}_{\text{P}}(\mathbf{r})} \sum_{i,j=1}^{N_m} \left\langle \epsilon_i(t)\epsilon_j(t) \right\rangle_t U_{i,j}(\mathbf{r}) \quad \text{with} \quad \mathcal{A}_{\text{P}}(\mathbf{r}) = \iint\limits_{R^2} P(\mathbf{u}+\mathbf{r})P(\mathbf{u})\,\mathrm{d}^2 u \tag{3}$$
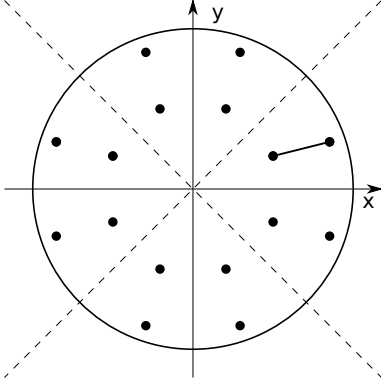

Figure 1: 8-fold symmetry of any couple of zonal modes (actuators).

where $\mathcal{A}_{\text{P}}$ is the pupil auto-correlation, $\left\langle \epsilon_i\epsilon_j \right\rangle$ is the temporal covariance of the DM commands residuals, i.e the residual wavefront as seen by the WFS, translated in DM modes (or commands) (without the tip-tilt modes) and $U_{i,j}$ is a special mixture of the DM's modes spatial covariance,

$$U_{i,j}(\mathbf{r}) = \iint\limits_{R^2} \left[h_i(\mathbf{u}+\mathbf{r}) - h_i(\mathbf{u})\right]\left[h_j(\mathbf{u}+\mathbf{r}) - h_j(\mathbf{u})\right]\,\mathrm{d}^2 u \tag{4}$$

We do not have a direct access to the covariance $\left\langle \epsilon_i\epsilon_j \right\rangle$, because it is affected by the WFS noise and spatial aliasing, and in the high bandwidth assumption (high loop frequency), Véran shows that

$$\left\langle \tilde{\epsilon}_i\tilde{\epsilon}_j \right\rangle = \left\langle \epsilon_i\epsilon_j \right\rangle + \left\langle n_i n_j \right\rangle - \left\langle a_i a_j \right\rangle \tag{5}$$

where $\tilde{\epsilon}_i$ is the residual DM command as measured by the WFS. We will now discuss the different components of this model.

Computing the $U_{i,f}$ functions Keck AO system is zonal, the modes are the DM's influence function, for which we have developed a totally empirical but highly accurate model.[7] These modes are used to build the high order structure function and the $U_{i,j}$ modes. In principle, because there are 349 actuators, there must be 61075 independent $U_{i,j}$ functions. But by exploiting the symmetries of all the couples of actuators (fig. 1), we can go down to 2655 truly independent functions - from which all the others can be built with a translation and a rotation. Overall, the computation of these functions requires about 1 min of CPU time. The possibility of using this approach is clearly an advantage of the zonal control as compared with the modal one. So we think that any PSF-R algorithm for any system should make use of a zonal basis, even if the system is modal by nature - it is indeed always possible to make a change of base, and in any case the DM control itself is generally zonal, so the actuators commands are accessible anyway.

2.2. The tip-tilt component

On the Keck-AO system, the tip-tilt is corrected with a dedicated tip-tilt mirror (TTM). The TTM command are two angles, from a quadratic projection of the reconstructed wavefront onto the x and y modes. We have verified that there is no tip-tilt left in the DM commands. The covariance between the tip-tilt and the influences function coefficients is zero for all practical purposes[†]. As a consequence, it is possible to build a stand alone tip-tilt structure function (which can be shown to be stationary anyway),

$$D_{\mathrm{TT}}(\mathbf{r}) = \frac{4\pi^2}{\lambda^2} \left[\sigma^2(\theta_x)\, x_{\mathrm{p}}^2 + 2\, \mathrm{cov}(\theta_x, \theta_y)\, x_{\mathrm{p}}\, y_{\mathrm{p}} + \sigma^2(\theta_y)\, y_{\mathrm{p}}^2 \right] \tag{6}$$

where θ_x and θ_y are the residual tip-tilt angles as seen in the telescope pupil, $\mathbf{r}_{\mathrm{p}} = (x_{\mathrm{p}}, y_{\mathrm{p}})$ are the coordinates in the pupil, and the wavefront tip-tilt structure function is translated into a phase structure function with the $2\pi/\lambda$ factor. Needless to say, the TTM commands are themselves also affected by noise $\tilde{\theta}_x = \theta_x + n_x$ and the noise is correlated between the two components. So, this noise will have to be removed before computing the TT structure function.

2.3. The LGS focal anisoplanatism component

Due to its nature - the difference between a flat and a spherical wavefront - the focal anisoplanatism (FA) error cannot be stationary across the telescope pupil. It has to have a quadratic behavior from the center to the edge of the structure function domain (i.e the OTF support). Now, in the context of our study, the LGS and the science object are always aligned, so the impact of the FA error on the long exposure OTF is necessarily circularly symmetric. Therefore, we believe that it must be possible to build an OTF FA filter that can be simply applied to the AO-OTF to mimic the effect of FA. So, in other words, we do not make any assumption about the stationarity anymore, but rather, pragmatically, claim that there exist an OTF filter that can do the same as FA is doing (and if the science object is off-axis, then there are good chances that an elliptical model would work.)
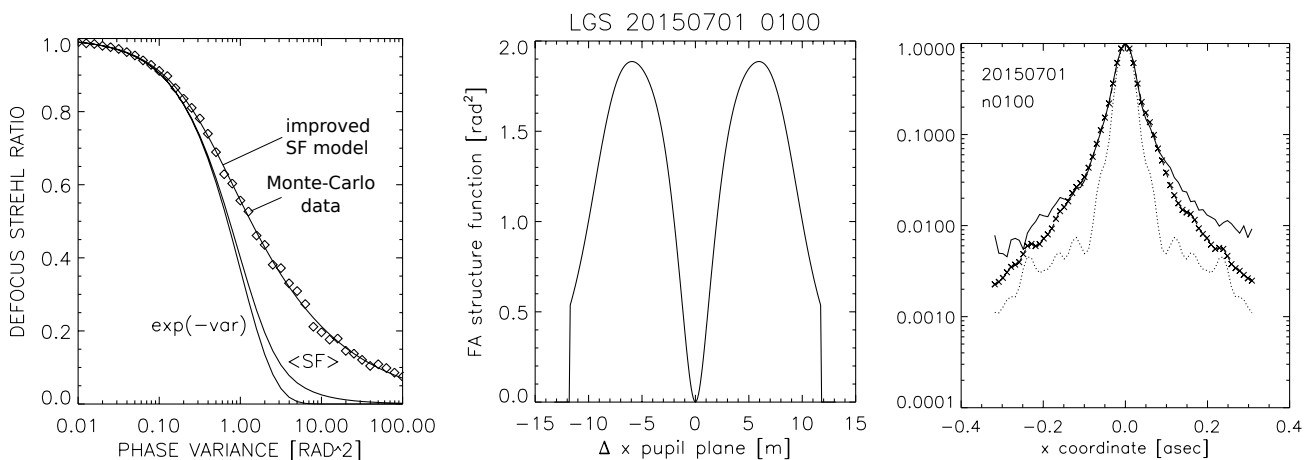

Figure 2: Left : Testing different defocus OTF models with the Strehl ratio as a function of the phase defocus variance. The diamonds are the results of a Monte-Carlo experiment and is the reference. We show the Maréchal model's prediction, the Strehl computed from the structure function averaged over the pupil ⟨SF⟩, and the Strehl computed from our empirical SF model (*improved SF model*). Middle : profile of the empirical structure function for one of the LGS observations (case 0100). Right : comparing the log profile of the sky PSF (cont.) the reconstructed PSF (crosses) and the reconstructed PSF **without taking the FA into account** (dots).

So, in order to continue with the OTF product paradigm, we needed an OTF filter model for FA. To get this, we made a series of optical turbulence Monte Carlo experiments of the FA error (i.e a flat turbulent phase minus

---

[†]theoretically we should see a correlation with the Zernike coma and some higher order terms - but most probably the tip-tilt components coming from other sources than turbulence dominate the signal.

a spherical turbulent phase), with defocus RMS values a_4 in the range 0-10 rad, and from the long exposure OTFs, we defined an equivalent OTF FA filter with the ratio

$$\text{OTF}_{\text{FA}} \equiv \frac{\text{OTF with FA error}}{\text{telescope OTF}} \qquad (7)$$

Using the relation $\text{OTF}_{\text{FA}} = \exp\left(-D_{\text{FA}}/2\right)$, we computed the associated structure functions, that we used as a basis to built our structure function empirical models, where the defocus RMS a_4 is the parameter.

Note that the approach we are following here is different from the approach consisting in averaging the non stationary defocus structure function across the pupil. By construction, our structure function automatically generates the correct overall OTF; while this is not the case with the averaged structure, which is accurate only in the weak phase situation, as figure 2 (left) shows. Here, we compare the focal anisoplanatism Strehl computed using three different methods : the Maréchal approximation $S = \exp{-\sigma_{a4}^2}$, the OTF computed from the averaged structure function, and our empirical SF model. Clearly, the empirical model follows very well the Monte-Carlo simulation results (the technical complexity of our model is not suited for this short proceeding and will be published in a more elaborate article on PSF-R for zonal systems.)

A profile of the FA structure function is shown in figure 2 (center), for one of the LGS cases. Our model simply uses as the scaling parameter the FA variance, computed from the C_N^2 profile and the system's geometry - telescope diameter and LGS altitude. In the same figure (right) we show what would be the impact of not taking the FA into account in the PSF reconstruction : one can see that FA is indeed a significant part of the whole error.

2.4. Focal anisoplanatism variance

There are several models available in the literature to compute the FA variance from the system's geometry, the laser beacon altitude and the C_N^2 profile - and we have evaluated two of them : Tyler's[10] and Parenti & Sasiela.[11] Tyler's approach is technically more challenging to implement, as it involves hypergeometrical functions - but these functions can be computed easily; Parenti & Sasiela approach is easier to implement, and this is what we are using :

$$\sigma_{\text{FA}}^2 = \int\limits_{h=0}^{\infty} C_N^2(h) \left[\frac{1}{2}\left(\frac{h}{h_b}\right)^{5/3} - 0.425\left(\frac{h}{h_b}\right)^2 \right] \mathrm{d}h \qquad (8)$$

where h_b is the height of the sodium beacon (LGS spot, about 90 km).

2.5. Optical turbulence structure function constant C_N^2 vertical profile

The C_N^2 profile we use comes from the measurements of a MASS[‡] profiler managed by the Mauna Kea Weather Center. Each night's data is archived and available at `mkwc.ifa.hawaii.edu`. There are some difficulties, though : (1) the MASS instrument is quite far from the telescope (300 m) and we do not know how the turbulent layers statistics varies laterally; (2) it is demonstrated[12,13] that MASS measurements are incorrectly estimating the layers strengths when the scintillation is strong, and we have no way of verifying if this is occurring; (3) the C_N^2 may evolve rapidly, but the MASS acquisition takes time so the profile corresponding to the time of observation is not necessarily available.

Because of these reasons, we believe there will be a net gain if the C_N^2 profile could be measured directly at the telescope, or at least within the telescope dome. A promising approach is the one proposed by Gilles & Ellerbroek[14] where the C_N^2 is reconstructed from the WFS data. It remains to be seen if this approach can be adapted to a single LGS case, though.

2.6. The LGS tip-tilt anisoplanatism component

Tip-tilt angular anisoplanatism is easy to model for a single guide star system. Tip-tilt is measured from a dedicated tip-tilt & defocus NGS somewhere close to the science target. From the angular separation vector between the NGS and the science target, and the C_N^2 profile, it is straightforward to compute the tip-tilt variances along and perpendicular to the separation vector, and include them into the tip-tilt structure function model given in Eq. 6. For this, we are using the tip-tilt variance model developed by Sasiela.[15]

[‡]Multi Aperture Scintillation Sensor

2.7. DM residual noise estimation

As we have seen above, the DM commands residuals ϵ_i are affected by the WFS noise and must be removed, because this noise component does not belong to the residual wavefront.

As far as we know there are two methods that can be used to assess the WFS noise from the WFS data[§] : (1) getting the noise level from a comparison of the WFS pixel data statistics with and w/o noise as proposed by Véran, and adapted by Jolissaint et al.[3] to SH systems; (2) adjusting noise power spectrums models, knowing the noise transfer function, on the WFS or DM commands data. The first approach is very efficient. Unfortunately, we do not have access to the raw pixel data in the case of the Keck system. Therefore we had to turn to the second option.

The noise on ϵ_i is coming from the WFS slopes measurements noise. Because each lenslet is associated with 4 actuators, the noise on ϵ_i **is correlated** from an actuator to the other. Therefore one has to develop a cross-spectrum model of the noise. But, assuming that the noise is white and knowing the loop transfer function, this is easy. The DM commands ϵ_i power spectrum have two components : the servo-lag error, and the noise error (see figure 3). The idea is to fit this two components model to the raw DM power spectrum, then extract the noise level.

There are nevertheless a few difficulties : (1) we need to know the C_N^2 and wind velocity profile to be able to build the servo-lag power spectrum. We have the first one, from the MASS, but not the second; (2) this model assumes that the phase is made of optical turbulence residual aberrations only, and we know that it is not the case : essentially, we always have a certain amount of unknown vibrations.

So, what we do is the following : we fit only the noise model, starting at a frequency where the contribution of the servo-lag and other errors are expected to be low - figure 3. Deciding on this frequency is done empirically. But it proves to lead to good results. Indeed, we have compared, for a few observations at different NGS brightness level, the predictions from a noise model formula used in AO errors budgeting,[9] and the measured noise, and the equivalence is remarkable.
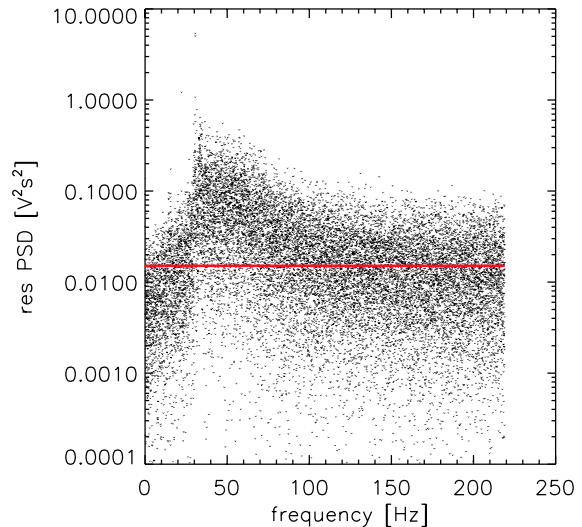

Figure 3: Estimating the white noise plateau level on the DM command power spectrum. The low frequency part shows the residual turbulence due to servo-lag and other low frequency errors, and the white noise generates the high frequency plateau.
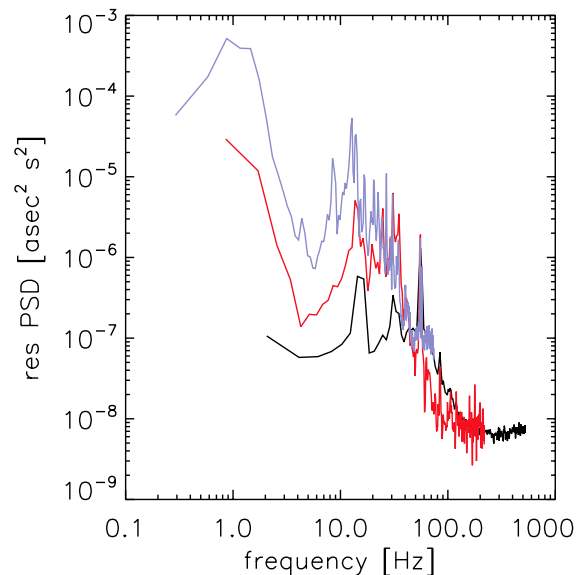

Figure 4: TT PSD for a loop frequency of 149 Hz (blue), 438 Hz (red) and 1054 Hz (black).

We have applied this technique to the tip-tilt signal - figure 4, but the noise plateau is less well defined, and there are peaks in the spectrums (vibrations) making the detection of the noise plateau difficult. A statistical analysis as we proposed in the point (1) above would be certainly beneficial for the tip-tilt noise estimation.

[§]here we cannot use noise models as used in budget error analysis, because we need the true noise of a given measurement
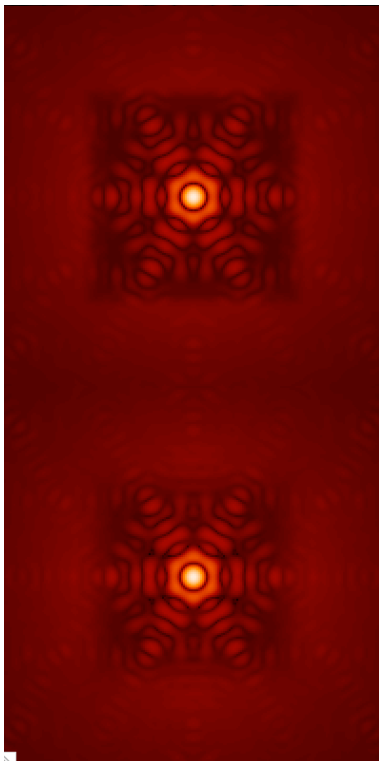
2.8. High order structure function

Figure 5: Top : long exposure PSF with a fitting error only using the Fourier approach; Bottom : the same using the MC approach.

There are two ways of computing the high order or so-called fitting error structure function : an analytical method, and a Monte-Carlo one.

The first method models the DM as a spatial filter that can remove the aberrations at all frequencies within the AO correction domain, set by the actuator pitch distance, $1/(2\text{pitch})$ - the exact shape of the domain will depend on the actuators' grid geometry. From this filter, we compute the residual Kolmogorov spatial power spectrum, then the structure function using a numerical Fourier transform. The difficulty is in establishing a realistic DM spatial filter, because the concept of spatial filter assumes that the correction is identical across the pupil, while it is actually not the case : the actuators are located at some fixed places. Our initial attempt was to simply assume that the DM filter is perfect, a square filter. The next attempt was to project the influence function basis onto the Dirac distribution,[9] and take the Fourier transform to get the spatial filter. But then the structure of the filter depends on the actuators grid location wrt the optical axis. We could have done an average, but this is not satisfactory.

The second method is a Monte-Carlo one : correction of turbulent phase screen with a DM basis model gives high order residual turbulent phase screens. The average of the spatial power spectrum of these residual, divided with the initial fully turbulent spatial power spectrum, gives the equivalent DM spatial filter. Note that instead of building a DM filter, Véran was simply directly computing the average high order structure function.

We have used the Monte-Carlo method. The two dimensional structure of the PSF at 1.22 μm, including the telescope diffraction structures, is shown in fig. 5. The square low order (or low frequency) aberrations domain where the phase is corrected is well apparent. The Fourier-based and MC-based PSF almost look the same, except that the transition between the corrected and uncorrected domain is smoother in the MC case.

Once the seeing from the run is known (from the DM commands), the fitting error structure function is build by (a) constructing the scaled Von Karman spatial power spectrum, (b) applying the DM spatial filter, then (c) computing the structure function from the residual power spectrum with a FFT algorithm.

2.9. WFS aliasing structure function

There are two aspects of the aliasing error : its theoretical description is quite complex, *but* it is weak relative to the other terms. Beside, when the guide star is faint and we have to lower the loop frequency, then aliasing gets lower, and servo-lag and noise error higher. Aliasing is therefore never really an issue, unless we want to get an exact model for it. So, what we have done is simply using a stationary assumption based model, allowing us to describe the aliasing as an additional low order spatial power spectrum added to the servo-lag error. From this aliasing power spectrum, the aliasing structure function is built. This purely analytic approach is detailed in Jolissaint.[9]

2.10. Deformable mirror based seeing monitor

(For details see Jolissaint et al..[5] This section is a mere summary.) As indicated in the introduction, the Fried parameter r_0 and the outer scale L_0 are obtained from the variances of the DM commands projected in the Zernike basis and compared to the Von Karman model.[16] Tip-tilt, defocus and astigmatism are not considered in the fit - they are affected by significant non-turbulent errors. Purely radial aberrations are left aside, because uncertainties on the actual value of the central obscuration makes the estimation

of these modes inaccurate. We are left with about 150 Zernike terms and this is enough to do an excellent fit to the Von Karman model. Overall, the Fried parameter we extract is in excellent agreement with the seeing estimated from seeing limited PSF observed in open loop with the same camera (NIRC2) - figure 6 - and with the typical outer scale values measured by other instruments at the Mauna Kea summit.

3. GETTING THE INSTRUMENTAL PHASE WITH ON-SKY PHASE DIVERSITY

Getting the non-AO part of the PSF, i.e the instrumental PSF, is the most difficult part of any PSF-R project. No point-like calibration source is available above the telescope, for obvious reasons. The aberrations are in principle generated by surface & alignment errors only, in principle the transmission of the optics is even across the pupils, but we have no way of measuring these individual errors during the AO run. We simply hope that these errors do not vary in time, which is certainly true, except for the alignments errors, which are changing with the telescope orientation. Actually, real static errors do not exist - they simply evolve slowly in time, at a slower rate than the turbulence aberrations. So it is more appropriate to talk about instrumental aberrations.

Figure 6: Seeing measured directly on an open loop PSF compared to the seeing extracted from the DM commands.

Getting a model of these aberrations for a complex system is hopeless - there are dozen of optical surfaces in the Keck+AO+NIRC2 system. They have to be measured as a whole, and, if we are able to determine the time scale of the instrumental aberrations, then a periodic measurement procedure must be set up.

We know two ways of measuring these aberrations. The one proposed by Véran consists in acquiring the image of a bright isolated single star in AO mode. If the AO correction is good, the assumptions we do in the PSF-R algorithm are valid, so the PSF-R must be accurate. So, we build the AO-OTF from the telemetry following the normal procedure, and **deconvolve** the (OTF of the) star image with this AO-OTF. What is left is the instrumental OTF. This is a simple procedure, ensuring that everything (all the instrumental aberrations) is taken into account in a single step. But we need to trust the AO-OTF reconstruction algorithm.

The second method - the one we use - is using a phase diversity procedure on sky sources. Basically, in AO mode, we acquire a focused and a defocused star image. On this couple of images, we apply a phase diversity procedure (we use the code provided by Mugnier et al.[17]) and get the phase that, **if it is located in the pupil**, generates the in/out-of-focus PSF we see. Now there is residual turbulence in the AO PSF, but fortunately the phase diversity code we are using is able to disentangle the part due to the structure of the imaged object and the part due to the phase. Residual turbulence structures are therefore seen as an object, and the code is able to converge. The assumption, though, is that these structures do not changes from the in-focus to the out-of-focus PSF acquisition ... now the seeing does change ! So we acquire a series of in/out-of-focus PSF, and select the couples for which the seeing is the same (using the DM seeing monitor).

Apart the seeing evolution problem, there is a limit to this procedure : these are no reason for the instrumental aberrations to be located only in the pupil. They are originating from all optical surfaces in the system. Therefore, if we propagate these aberrations in the pupil plane, they will generate a phase **and** and amplitude aberration. Therefore, what is needed is not only a phase diversity procedure, but instead a **phasor diversity**, and ONERA team (private comm.) has developed such a tool, which makes use of three defocused PSF instead of one. We do not have access to such a tool yet, what we are doing is a phase-based only instrumental aberrations reconstruction. Fortunately our reconstructed instrumental PSF looks very close to the sky PSF (beyond the residual turbulence structures).
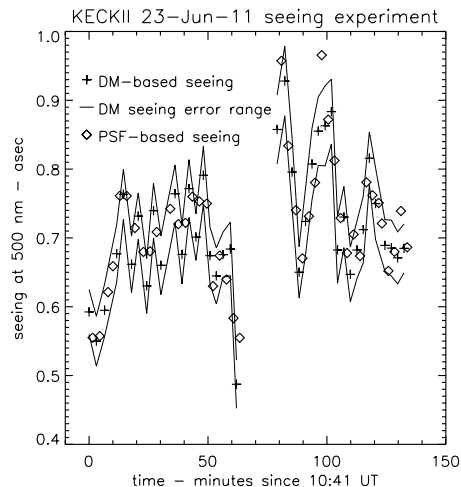
4. PSF RECONSTRUCTION - ON-SKY TESTS

Since the beginning of the project, 30 data sets, several thousands of NGS and LGS data, have been taken, each of them allowing some progress on the algorithm development. The four data sets below are the ones for which a convergence has been reached in the tool development. So, future PSF-R algorithms developers do need to realize that developing and testing such a tool **requires hundreds of hours of telescope time** to reach some level of maturity.

4.1. NGS case 20130203 - 3 February 2013
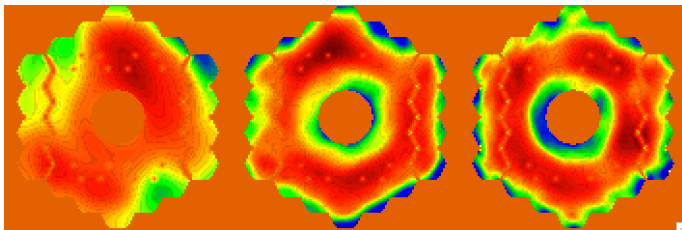
Figure 7: From left to right : reconstructed instrumental phase for 2, 4 and 6 mm of defocus. The WFE RMS are respectively 74, 94 and 98 nm; the P2V are 354, 483 and 463 nm.

The first difficulty we had to face was to make sure we had the correct information on the reference frame change (rotation, flip) to go from the focal plane (the detector is NIRC2) to the telescope pupil plane. This verification actually required several data sets, test with calibration source, the DM, etc. This simple issue took a lot of effort.

Matching different in/out-of-focus PSF - for the phase diversity procedure - according to the seeing value was not a difficulty. We had defocus values of 2, 4 and 6 mm. The optimal value being 4.5 mm according to the phase diversity tool user manual.
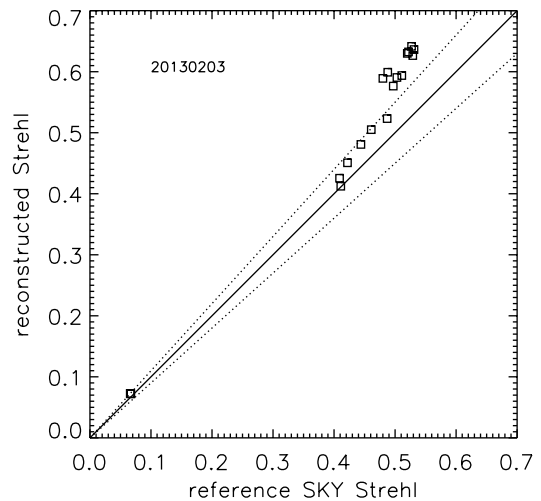
The 2 mm value was clearly too low but the associated reconstructed static PSF had the best match with the sky PSF. The 4 and 6 mm were giving a better match in term of Strehl, and the PSF structure was still compatible with the sky PSF. We finally considered for the static phase a scaled value of the 2 mm case, using the 4 mm and 6 mm cases WFE RMS. This is a typical example of what needs to be done - sometime - to get a satisfactory instrumental PSF. The WFE we got was 96 ± 2 nm - figure 7.

The reconstructed Strehl (instruments and turbulence) is compared with the sky Strehl in figure 8. The sky Strehl is computed from the PSF, using a Strehl-meter developed by Marcos Van Dam. As this metrics is extremely important for our project, we did an independent estimation of the Strehl using our own procedure. What we found is that amongst all the sky PSF for all the NGS cases, the correlation was excellent, more than 0.99, with no intercept. The RMS of the relative difference between the two methods was 10% so we decided to take this 10% as an estimate of the accuracy of the sky Strehl determination.

This $\pm10\%$ is shown as a dotted line in figure 8. It shows that most of the reconstructed Strehl are compatible with the sky Strehl, except for a group of data points. These points correspond to the NGS we used for the phase diversity. They were very bright, and the loop frequency was set to 1054 Hz. In principle, when the star is bright, the PSF-R is working in a regime where the assumptions we do in the theory are valid. Now, for the dimmest star of this data set, one can see that the reconstructed Strehl matches well the sky Strehl. So, the behavior of the reconstruction error does not follow the intuition. There must be something special in bright NGS conditions, requiring some investigations.

Figure 8: Reconstructed versus sky Strehl ratio for the data set 3 February 2013. Fe-II filter (1.646 μm).

Nevertheless, overall, the trend is excellent. We show in figure 9 a comparison of the profile of the reconstructed and sky PSF for a bright (630 photons/lenslet/ms), a medium bright (141 photons/lenslet/ms) and a dim NGS (20 photons/lenslet/ms). Figure 10 shows a 2D and 3D PSF comparison.
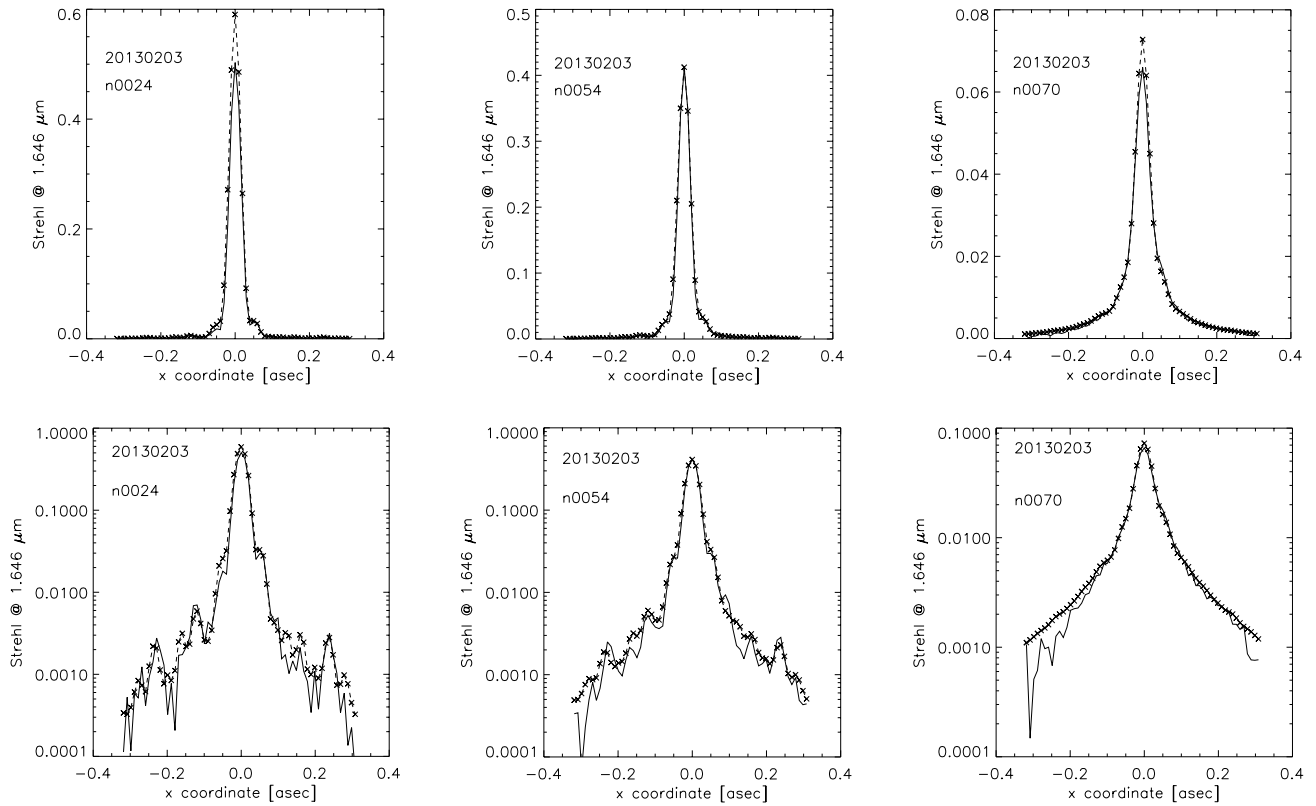
Figure 9: Left to right : reconstructed PSF for a bright, medium and dim NGS (case 20130203, see text) as compared with the sky PSF (continuous line). Top line shows the linear profile, bottom line a log profile.
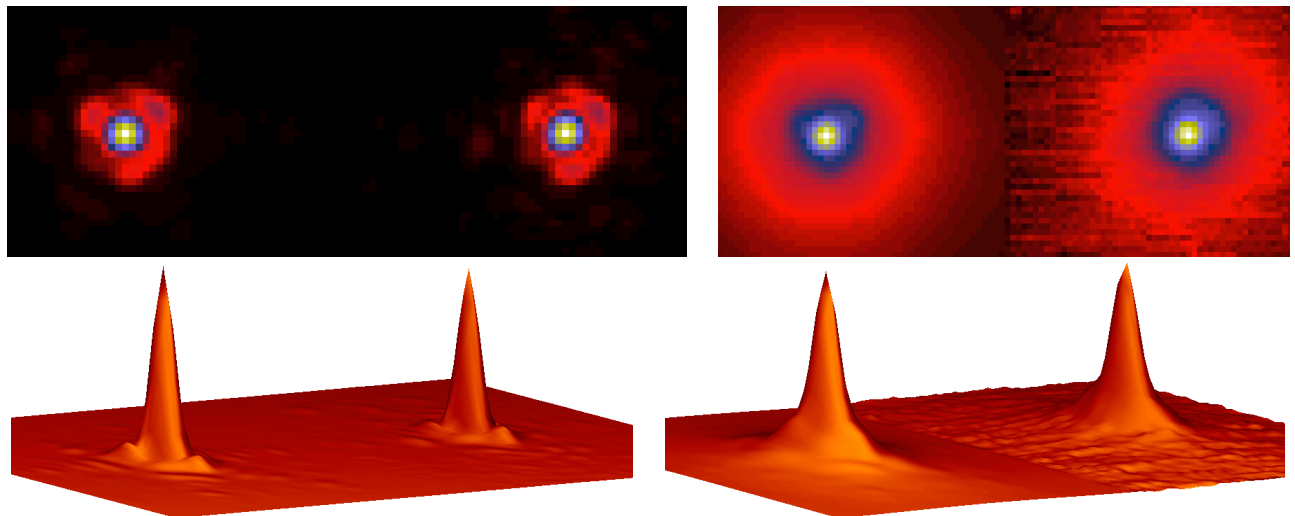

Figure 10: Two and three dimensional PSF profiles compared. Left : case 0024 (bright NGS); right : case 0070 (dim NGS). On each figure, the sky PSF is on the right.

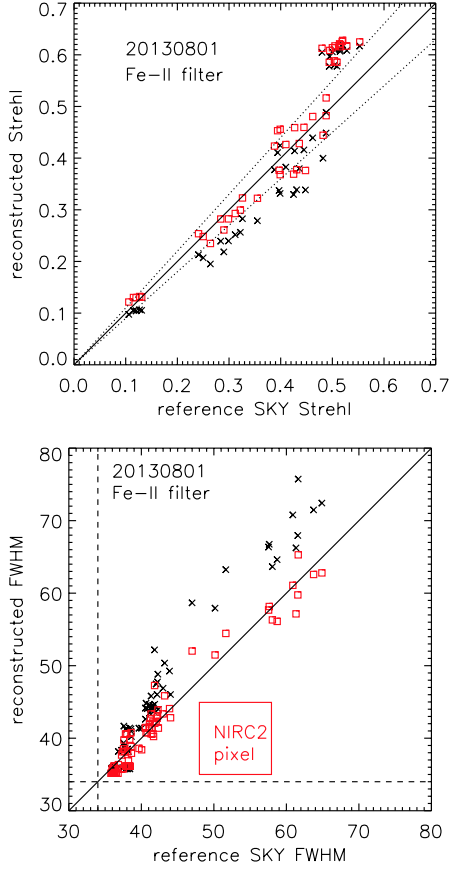## 4.2. NGS case 20130801 - 1st August 2013

Figure 11: Top : Reconstructed vs. sky Strehl for the data set 20130801. Bottom : PSF FWHM comparison. Fe-II filter (1.646 μm). Black points are before correction of the excess of tip-tilt, red points after.

This set is interesting as it demonstrates the impact of possible non common path aberrations (vibrations) on the reconstruction. When comparing the FWHM of the reconstructed and sky PSF - figure 11, bottom - we saw a systematic excess in the reconstructed one. We were able to realize that this excess was coming from the tip-tilt. Indeed, when compared to the sky PSF FWHM, the tip-tilt RMS given by the WFS measurement was larger. So, the WFS was sensing more tip-tilt than what was actually seen on the sky. This discrepancy was also apparent on the reconstructed Strehl (same figure, top).

Assuming that the issue was coming from an excess of tilt, we removed some amount of tilt RMS by down-scaling the tip-tilt structure function amplitude, by a multiplicative factor of 0.7 ($\sqrt{0.7} = 0.84$). This meant that 16 % of the tip-tilt seen by the WFS was coming from an other source than turbulence, and was not common with the DM arm. The consequence of this correction was to remove also the Strehl discrepancy.

Once again, we can see in the Strehl plot that there is a systematic error of the reconstruction for the brightest stars, again the ones we took for the phase diversity (see the top-right cloud of points in the Strehl plot). It seems obvious that a parameter is changing when the NGS are bright, a parameter that we do not capture. Interestingly, these data do not seem to be affected by the tilt problem, because the corresponding points in the Strehl plot have changed much less than the others.

The reconstructed instrumental phase did not change much during the data acquisition. The structure looks the same (not shown here, but close in shape to the figure 7) and the WFE RMS was in the range 157 nm to 132 nm.

We show in figure 12 and 13 a selection of a few good reconstruction cases.

4.3. NGS case 20130914 - 14 September 2013

The reconstructed instrumental phase was in line with the previous case, one month earlier, but varied across the night - from 95 to 165 nm. Therefore, we should have considered different cases of instrumental phase for the different reconstructed PSF. The reconstructed PSF Strehl is approximately 20% higher than the sky Strehl, and we do not have an explanation yet for this, except a possible error in the static phase estimation.

What is interesting with this example is that the reconstruction error is on the other direction than with the previous cases. For one set the reconstruction seems too pessimistic, and for an other, too optimistic. A conceptual flaw in the algorithm would probably generate a persistent error scheme, regardless of the data acquisition conditions. We think that more data is required to have a clear statistical understanding of the algorithm accuracy.

4.4. LGS case 20150701 - 1st July 2015

These PSF data were taken with the recently implemented center launch system using the dye laser. 60 PSF were acquired in LGS mode. The PSF acquisition for the phase diversity was done in NGS mode, on a bright star. The reconstructed phase shape was somewhat different from the previous static phases found in 2013, almost two years earlier. But the system experienced a significant realignment between these dates. The WFE
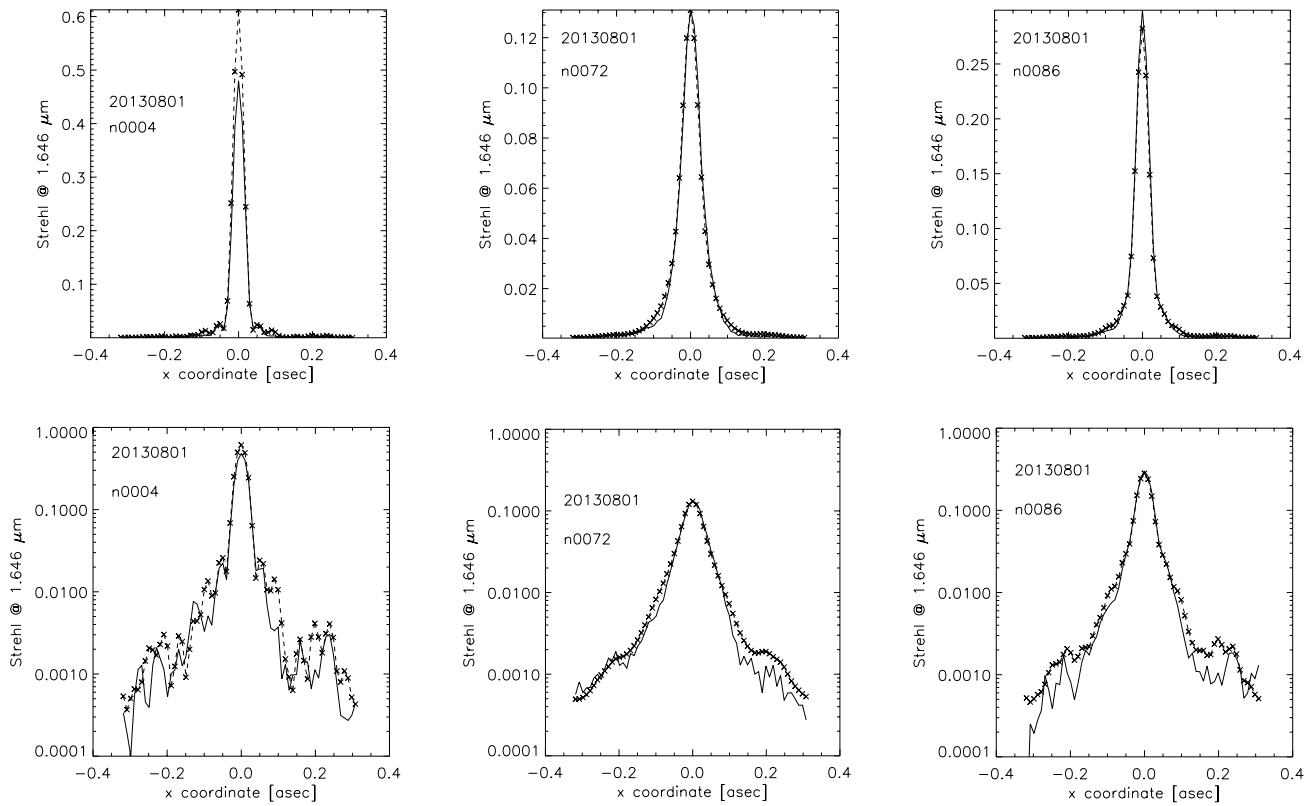
Figure 12: Left to right : PSF reconstruction for a bright, medium and dim NGS (case 20130801, see text) as compared with the sky PSF (continuous line). Top line shows the linear profile, bottom line a log profile.
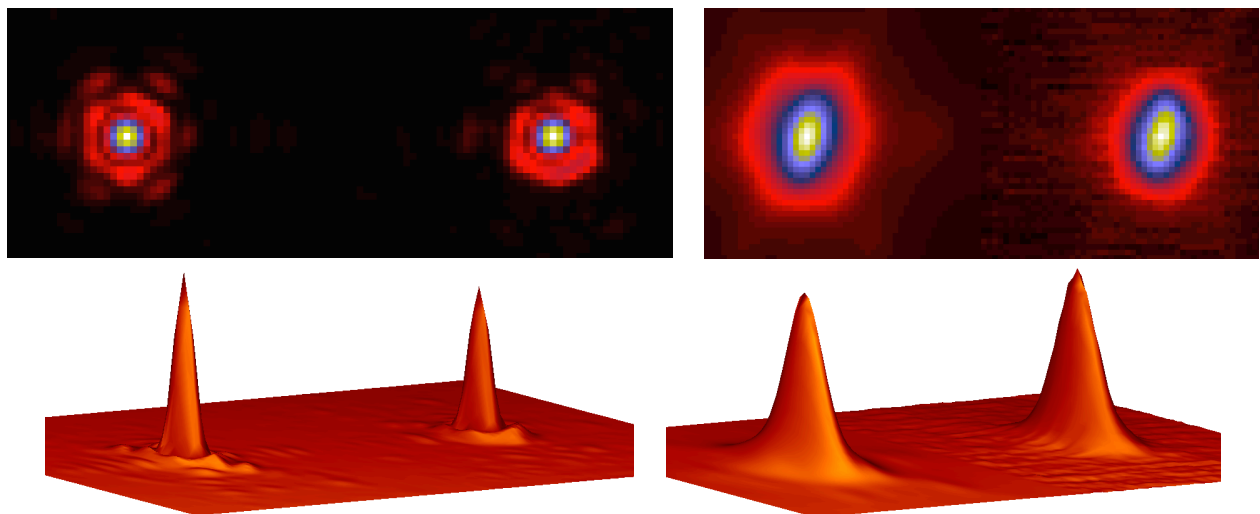

Figure 13: Two dimensional and three dimensional PSF profiles compared. Left : case 0004 (bright NGS); right : case 0072 (dim NGS). On each figure, the sky PSF is on the right.
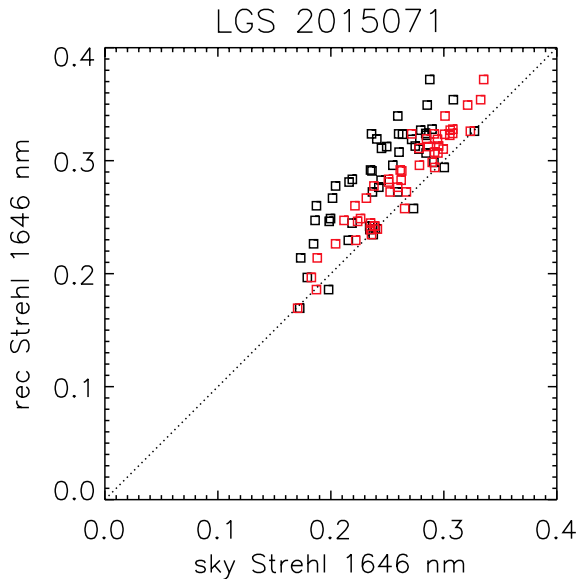
Figure 14: Comparison of the reconstructed and sky Strehl using two types of sky PSF energy normalization (see text). The white squares correspond to a normalization to the same level of energy with the PSF core, and the red squares to a best fit of the sky PSF profile with the reconstructed one.
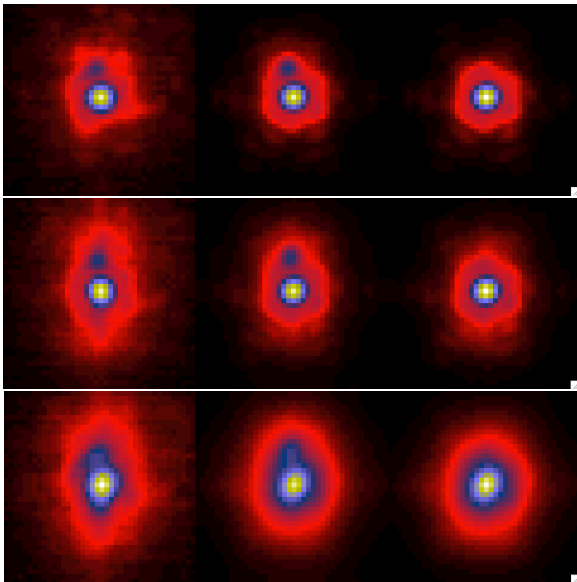

Figure 15: For the cases 0107, 0069, 0098 of the LGS set, from left to right : the sky PSF, the reconstructed binary model using the reconstructed PSF, and the reconstructed PSF. All images Fe-II filter. Field-of-view 0.4".

RMS was 91 nm, quite negligible wrt the residual turbulent WFE we should expect in LGS mode (about 300 nm according to our WFS measurements).

The sky PSF were showing lots of residual (turbulent ?) structures which made the Strehl estimation rather inaccurate. In fact, a persistent structure just above the main PSF core made us believe that the test star was actually a **binary**.

We normalized the sky PSF to the same amount of energy than the reconstructed PSF within a radius of 11 pixels, which corresponds to where the sky PSF profile reached the background level. A companion star would only change the normalization by a common factor. The correlation of the reconstructed Strehl with this sky Strehl was 79% - see figure 14. In a second test, we made a scaling of the sky PSF to get the best profile fit with the reconstructed one, again within a disc of 11 pixels in radius. In this case, the Strehl correlation went up to 96 % (same figure, red squares). The reconstructed Strehl, though, is slightly higher than the computed sky Strehl, 16% in the first normalization and 7 % for the second. This might simply be an effect of the companion.

In any case, it is important to keep in mind what a reconstructed PSF is used for : finding a model of the PSF profile to allow for astrometric and photometric analysis, and deconvolution. In these cases, the actual PSF amplitude (or Strehl) is not a useful parameter. The Strehl comparison we like to do is only to test the quality of the reconstruction, because it is immediately related to the WFE, a quantity that has a physical meaning. To conclude, the fact that when adjusting the sky and reconstructed amplitude to get the best profile match we find a Strehl correlation of 96 % demonstrate that the PSF we reconstruct with our algorithm might have some interest for AO data reduction.

We actually used the reconstructed PSF to fit a binary star model to the sky images, and did find a systematic separation of 60 masec ± 5 masec, and an intensity ratio of approximately 0.13 - figure 15. Of course, we could not exclude that this feature was a PSF aberration, but on the K-band images of the same star (we have three K-band LGS PSF) this feature was not apparent anymore. If it was a wavefront error, then its position wrt the central star should have been proportional to the wavelength (i.e located at 80 masec separation). In K-band, the companion image was burden into the central star peak.

This did not prevent us to compare the PSF profiles, in a direction perpendicular to the separation vector with the companion. We show in figure 16 a comparison of the log profile of the reconstructed and sky PSF (the normalization is such that there is the same amount of energy in the core of both PSF).
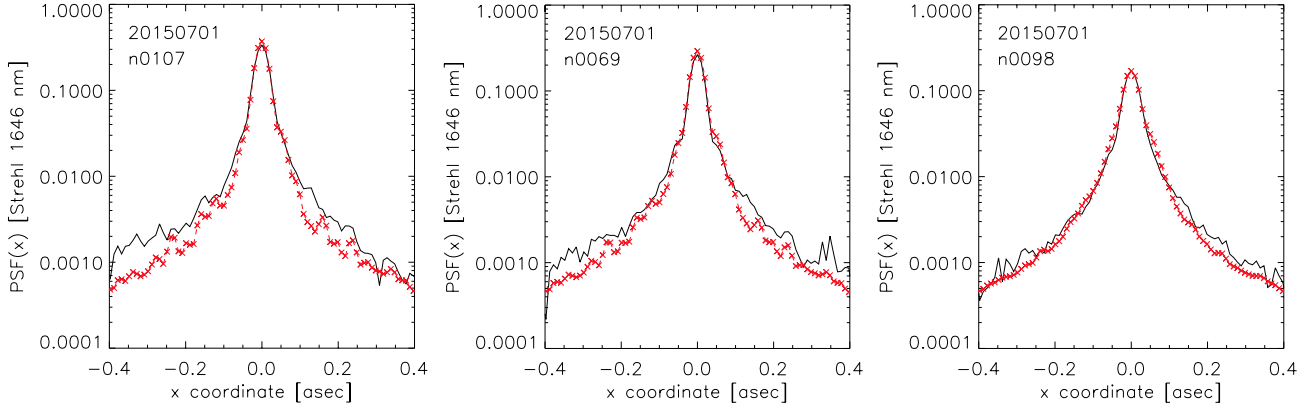
Figure 16: Left to right : sky (continuous line) and reconstructed (red) PSF profile comparison for three of the 60 cases. The reconstructed Strehl is respectively 0.37, 0.29 and 0.17, in Fe-II filter.

5. WHAT WE HAVE LEARNED : A SUMMARY

There are many aspects in a PSF reconstruction program. This Keck project took several years to complete, and a very large amount of sky data and telescope time, sometime just to verify that our assumptions about the system geometry dimensions were right (central obscuration diameter, detector vs. DM vs. pupil orientation, etc.) It is certainly impossible to make a complete summary in a short conference proceeding as this one, and we will simply try to mention the most important point to us, and, also, what we think must be the next steps.

- there is absolutely no doubt that one of the most difficult task is to get the instrumental phasor. We are specifically talking about the phasor here because both the phase **and** the amplitude in the pupil must be known. It is nevertheless always possible to use a phase-only reconstruction algorithm, because any phase diversity algorithm will always converge to **some** solution, but there is no certainty that the PSF we derive from this phase is valid. A phasor diversity algorithm must be developed for a full PSF-R. This can be done (Mugnier et al. developments) and we have proven that as long as the seeing can be measured with a good accuracy, star images in AO mode can be used as sources. Of course, the time scale over which the instrument phasor must be re-acquired depends on the specific stability conditions of the observatory and instruments. Ideally, once every AO night would be sufficient, but our experience shows that static aberrations do change during the night. *Last minute note* : the reflectivity of each of the Keck telescope segments is known. Including this knowledge in the phase diversity algorithm should clearly improve the solution.

- getting the seeing is relatively easy using the DM commands, as we have shown. But what is more critical is to get the C_N^2 profile. In our experiment it was taken from a MASS instrument about 300 m from the telescope, with no certainty on the validity of this measurement at the telescope location - it is probably valid, because the layers that are important in the focal anisoplanatism error are the high altitude layers, but a local measurement of the profile, from within the telescope dome, or even using the WFS measurements would be preferable.

- NCPA : aberrations not common to the DM and the WFS arms are an issue for PSF-R, as we use the WFS measurements to determine the residual seen at the DM level. In particular, non common path vibrations can have a strong impact.

- telemetry : in some cases along our experiments, telemetry data was totally corrupted and of no use. As end users of the telemetry, we had no way of knowing what went wrong with the telemetry recording. Besides, there must be absolutely no limit in any data acquisition and access. In PSF-R, every detail is important. In particular, it is highly desirable to get the full record of the raw WFS pixel data. This gives the total freedom of the choice of the method to use to assess the WFS noise contribution.

13

- control system parameters : (loop gain etc.) an AO system is a complex system, with many calibration and scaling parameters between the sub-systems. Knowing the values of these parameters is obviously extremely critical when one wants to translate - for instance - a DM command given in volts into microns. But these parameters are not always easy to find, and they might even not be documented !

- the stationary assumption we use all along our developments is very convenient as it allows first to handle separately the different sources of aberrations, and second to make the whole computation very fast (less than a minute, instead of an hour without the assumption). When looking at the residual variance maps in the pupil, the good news is that stationarity is actually a fact, rather than an assumption. Only on the edges can we see some increase of the residual. On an extremely large telescope, because the surface becomes so large relative to the edges, the stationarity might become even more pronounced. Then, if we use a zonal description, we can make use of the symmetries of the couples of actuators inside the pupil, and keep the whole computation time really reasonable, mostly independent of the telescope diameter.

- going off-axis : the geometry of a single GS system in LGS mode is simple. Off-axis focal anisoplanatism is the result of the difference between a flat wavefront in a cylinder on a spherical wavefront inside a cone, where the axis of the cylinder and the cone have an angle. It must be possible to model this effect using an elliptical SF model, possibly using an empirical approach as we did for the on-axis case.

- the next steps in the project : our algorithm seems to produce good results, and the only way to move further in the development is to make a statistical analysis of the reconstruction quality. For this, more NGS/LGS data are needed. Systematic errors would then appear, that we could interpret in term of structure function or anything else, and try to improve the algorithm. But the science teams can start to use the PSF-R code right now, and verify if it brings any gain in the quality of the data reduction.

6. ACKNOWLEDGEMENTS

REFERENCES

1. S. Ragland, L. Jolissaint, P. Wizinowich, J. Chock, J. Mader, M. R. Morris, and S.Kwok "Point spread function determination for Keck adaptive optics (AO4ELT-4 Conference proceedings, February 2016)," *this conference*, 2016.
2. J.-P. Véran, F. Rigaut, H. Maître, and D. Rouan, "Estimation of the Adaptive Optics Long-exposure Point Spread Function using Control Loop Data," *Journal of the Optical Society of America A* **14**, pp. 3057-3069, 1997.
3. L. Jolissaint, J.-P. Véran, and J. Marino, "OPERA, an automatic PSF reconstruction software for Shack-Hartmann AO systems: application to Altair," in *Astronomical Telescopes and Instrumentation*, *SPIE Proceedings* **5490**, pp. 151-163, 2004.

4. L. Jolissaint, J. Christou, P. Wizinowich, and E. Tolstoy, "Adaptive optics point spread function reconstruction: lessons learned from on-sky experiment on Altair/Gemini and pathway for future systems," in *Astronomical Telescopes and Instrumentation, SPIE Proceedings* **7736**, pp. 77361F-77361F-12, 2010.

5. L. Jolissaint, C. Neyman, J. Christou, P. Wizinowich, and L. M. Mugnier, "First Successful Adaptive Optics PSF Reconstruction at W. M. Keck Observatory (AO4ELT-2 Conference proceedings, Sept. 2011)," *eprint arXiv* **1202.3486**, 2012.

6. L. Jolissaint, L. M. Mugnier, C. Neyman, J. Christou, and P. Wizinowich, "Retrieving the telescope and instrument static wavefront aberration with a phase diversity procedure using on-sky adaptive optics corrected images," *SPIE Proceedings* **8447**, article id. 844716, 2012.

7. L. Jolissaint, C. Neyman, J. Christou, and P. Wizinowich, "Adaptive optics point spread function reconstruction project at W. M. Keck Observatory: first results with faint natural guide stars," *SPIE Proceedings* **8447**, article id. 844728, 2012.

8. L. Jolissaint, S. Ragland, P. Wizinowich, and A. Bouxin, "Laser guide star adaptive optics point spread function reconstruction project at W. M. Keck Observatory: preliminary on-sky results," *SPIE Proceedings* **9148**, article id. 91484S, 2014.

9. L. Jolissaint, "Synthetic modeling of astronomical closed loop adaptive optics," *Journal of the European Optical Society: Rapid publications* **5**, p. 10055, 2010.

10. G. A. Tyler, "Rapid evaluation of d_0: the effective diameter of a laser-guide-star adaptive-optics system.," *Journal of the Optical Society of America A* **11**, p. 325, 1994.

11. R. R. Parenti and R. J. Sasiela, "Laser guide-star systems for astronomical applications," *Journal of the Optical Society of America A* **11**, p. 288, 1994.

12. E. Masciadri, G. Lombardi and F. Lascaux, "On the comparison between MASS and generalized-SCIDAR techniques," *MNRAS* **438**, p. 983, 2014.

13. G. Lombardi and M. Sarazin, "Using MASS for AO simulations: a note on the comparison between MASS and Generalized SCIDAR techniques," *MNRAS* **455**, p. 2377, 2016.

14. L. Gilles and B. Ellerbroek, "Real-time turbulence profiling with a pair of laser guide star Shack-Hartmann wavefront sensors for wide-field adaptive optics systems on large to extremely large telescopes," *Journal of the Optical Society of America A* **27**, 26, p. A76, 2010.

15. R. J. Sasiela, "Wave-front correction using one or more synthetic beacons," *Journal of the Optical Society of America A* **11**, p. 379, 1994.

16. D. M. Winker, "Effect of a finite outer scale on the Zernike decomposition of atmospheric optical turbulence," *Journal of the Optical Society of America A* **8**, pp. 1568-1573, 1991.

17. L. Mugnier, J.-F. Sauvage, T. Fusco, A. Cornia and S. Dandy, Optics Express, **16**, (2008), 18406-18416